

Thermal transport through thin films: Mirage technique measurements on aluminum/titanium multilayers

E. J. Gonzalez, J. E. Bonevich, G. R. Stafford, G. White and D. Josell
National Institute of Standards and Technology, Gaithersburg, MD 20899

ABSTRACT

Thermal transport properties of multilayer thin films both normal and parallel to the layers have been measured. Al/Ti multilayer films 3 μm thick, with individual layers systematically varied from 2.5 nm to 40 nm, were studied on Si substrates. Layers of Al and Ti were nominally equal in thickness, with actual composition determined for each specimen using energy dispersive spectroscopy. The thermal diffusivity both in the plane and normal to the plane of the films (thermal conductivity divided by specific heat per volume) was found to decrease significantly with decreasing bilayer thickness. Pure Ti and Al films as well as Cu films from 0.1 to 5 μm thick were also studied. In plane electrical conductances of the Al/Ti multilayers were also measured.

INTRODUCTION

It is generally recognized that thermal transport properties of thin films can be less than half those of bulk materials [1, 2, 3, 4]. This decrease can arise from modifications within the bulk of the films (i.e., high defect density or low mass density) or an interface thermal resistance. A comprehensive examination of the latter effect can be found in review articles by Swartz and Pohl [5] and Cahill [6]. Some researchers have measured the interface resistance by studying the thermal transport properties of metal/metal [7, 8], metal/oxide [9], oxide/oxide [10] or semiconductor/semiconductor [11, 12, 13, 14, 15, 16] multilayer films. Unlike techniques using single layer films, experiments using multilayers can separate interface effects from those due to total film thickness, e.g. systematic measurement errors. Discussion and analysis of experimental data utilizing models of the scattering at the interfaces exist in the literature [17, 18, 19].

To our knowledge, this work is the first time that anisotropic thermal transport properties of multilayer thin films have been measured using the Mirage technique; the only other published measurement of anisotropic properties was accomplished using ac-calorimetry [15]. By studying films with a range of bilayer thickness, it has been possible to systematically examine the effect of the interfaces on the anisotropic thermal diffusivity. Most of the cited studies used techniques that restricted their measurements to in-plane thermal diffusivities, though a few used transient reflection [8, 16] or transmission techniques [7, 9], or simplified mirage [12] that were limited to studying the diffusivity normal to the film surface. The Mirage technique utilized here is capable of measuring the thermal diffusivity at room temperature in both the normal and in-plane directions.

The theory for the Mirage technique measurements used here has been outlined in several publications [20,21,22], including a later correction [23] of the theory required due to errors in the earlier analyses. In this technique, a focused *heating* laser aligned normal to the specimen surface is used to heat a spot on the surface of the specimen (see Fig. 1). Temporal modulation of the laser intensity results in oscillatory temperature distributions both in the body of the sample and on its surface. A second *probe* laser aligned nearly parallel to the specimen surface is deflected by these temperature oscillations and the vector amplitude and phaselag (relative to the modulated heating laser) of that deflection is recorded as a function of the horizontal distance

between the pulse and probe lasers (see Fig. 1). Like a mirage in the desert, this deflection is caused by gradients in the index of refraction of the air arising from temperature gradients induced by the temperature oscillations on the specimen surface. The data are fitted to solutions of the 3-dimensional thermal diffusion equations for the ambient/specimen/ambient geometry with appropriate boundary conditions on heat flux and temperature continuity [21-23]. The fitting routine uses a multiparameter least-squares-fitting procedure to optimize the fit. Because the experiment utilizes oscillatory heating, it is most sensitive to the thermal diffusivity α . The thermal diffusivity equals the thermal conductivity κ divided by the specific heat per unit volume of material C_v , $\alpha = \kappa \cdot C_v^{-1}$. If the thermal conductivity is anisotropic, then the thermal diffusivity α^* in a particular direction, is given, in terms of the thermal conductivity κ^* in that direction, by $\alpha^* = \kappa^* \cdot C_v^{-1}$. For the materials studied here, which have rotational symmetry about the specimen normal, the only unique values of thermal conductivity are those in the normal direction, κ^\perp (thermal diffusivity α^\perp), and in the in-plane direction, κ^\parallel (thermal diffusivity α^\parallel). Hereafter, the conductivities and diffusivities are understood to be the thermal transport properties.

A detailed description of the particular experimental apparatus can be found elsewhere [21-24]. The experimental data for each specimen are amplitudes and phases of both the normal and the transverse components of the probe beam deflection, relative to the specimen surface, as functions of horizontal displacement. Each specimen was studied using three different modulation frequencies, in the range 20 to 40 kHz, for the heat source. Amplitude and phase signal obtained from one specimen at one of the three frequencies is shown in Fig. 2. Data at the other test frequencies are qualitatively similar in appearance, though the relevant length scale changes with the test frequency.

EXPERIMENTAL PROCEDURE AND DATA

Single Layer Thin Films

Monolithic specimens have been studied using this apparatus; values of thermal diffusivity obtained for bulk Si, Cu, Al₂O₃ and Inconel [24,25] are in good agreement with accepted values. A limited study of oxide film on substrate specimens has also been published [22]. However, the range of film thickness for which the apparatus and technique are reliable for studying metallic films on substrates has not been established. To this end, single layer Cu films between 0.1 μm and 5 μm thick were studied. The films were fabricated using an electron beam evaporator source (99.99% purity) in a system with base vacuum $< 2 \times 10^{-6}$ Pa, and operating vacuum in the mid 10^{-5} Pa range. In order to ensure good adhesion, the quartz substrates were sputter cleaned in-situ using Ar ions and coated with approximately 1 nm of Ti prior to deposition of the Cu films. The measured diffusivity of the 0.5 μm and thicker Cu films is isotropic and approximately 10% lower than the value obtained from bulk specimens (and the literature value) in their as-deposited state (Fig. 3) [26]. To test the possibility that high defect density was the source of the difference, the films were annealed at 400 °C for 4 hr in an Ar-5% H₂ mixture and remeasured. The results of tests on as-deposited and annealed specimens are summarized in Fig. 3.

Monolithic Al (and Ti) thin films, also 3 μm thick and deposited on borosilicate glass and Si wafers, were studied. The measured diffusivity and conductivity are reported in Table I and compared with literature values [26, 27]. The diffusivity of the Al films agrees with reported bulk values, and no anisotropy was detected. The diffusivity of the Ti film, on the other hand, is

approximately 1/3 of the literature value $0.0925 \text{ cm}^2 \cdot \text{s}^{-1}$ (Table I). To understand the source of this difference, the diffusivity of the (bulk) source Ti used for the deposition was also measured. The measured value of $0.0775 \pm 0.002 \text{ cm}^2 \cdot \text{s}^{-1}$ is significantly below the bulk value (uncertainty represents the root-mean-square variation of three independent measurements). This result seems inconsistent with the 99.7% purity of the source Ti. However, as is standard for such materials, this number represents only the metallic impurity content. The low measured diffusivities may represent the effects of other impurities, e.g. hydrogen or oxygen in solution.

Multilayer Thin Films: Thermal Diffusivity

Multilayer thin films composed of alternating layers of Al (99.99%) and Ti (99.7%) were deposited on Si wafer using the same deposition system used to deposit the Cu films. Specimens were fabricated with nominal layer thickness of 2.5 nm, 5.0 nm, 10 nm, 20 nm, and 40 nm. The total thickness of all films was maintained the same, nominally $3 \mu\text{m}$, obtained by adjusting the number of layers accordingly. Furthermore, all films had nominally equal Ti and Al layer thickness. The actual bilayer thickness of each specimen was obtained from low and high angle x-ray diffraction satellites as well as transmission electron microscopy (TEM) as shown in Fig. 4 and Ref. [28]. The actual ratio of Al to Ti was obtained from energy dispersive x-ray spectroscopy utilizing elemental standards. The experimentally determined bilayer thickness, total film thickness, and composition for all specimens are shown in Table II.

The results for the multilayer films indicate significant anisotropy of the thermal transport properties. This is not surprising for a layered structure of two materials with dissimilar diffusivities. The measured diffusivity values normal and parallel to the layers, i.e. normal diffusivity and in-plane diffusivity, respectively, are summarized in Fig. 5. In order to compensate for the slightly different compositions of the multilayers (Table II), experimental values have been normalized by the values (normal and in-plane diffusivities) predicted for each specimen. For the predicted values, the Al and Ti layers were modeled as thermal conductors in parallel (in-plane) and thermal conductors in series (normal). The measured thermal transport properties of the pure $3 \mu\text{m}$ films of Al and Ti (Table I) and relative layer thickness (from the compositions in Table II) were used. Note that interface effects are neglected in these geometry-based predictions.

Multilayer Thin Films: Electrical Conductivity

The in-plane electrical conductances of the multilayer films were obtained using a four-point probe technique [29]. The results of those experiments are summarized in Fig. 6 (total fractional uncertainties are estimated to be less than 1% of measured values).

ANALYSIS AND DISCUSSION

Cu Films

The diffusivities of all the Cu films increased during annealing (Fig. 3), with that of the thickest film falling within 5% of the bulk value. Plane view SEM micrographs were obtained from the $5 \mu\text{m}$ thick film in the as-deposited and annealed states (Fig. 7). The micrographs show that significant grain growth occurred during annealing. These results demonstrate both the sensitivity of the Mirage measurement technique and the impact of the microstructure on the transport properties.

Assuming that the change of the diffusivity of the Cu films is due to reduction of grain boundary area and associated thermal resistance, an average grain size for the as-deposited films is calculated using the measured values and the expression,

$$\frac{t}{\kappa_{\text{exp}}} = \frac{t}{\kappa_{\infty}} + \rho \quad (1)$$

κ_{exp} is the conductivity of the film (determined from the measured diffusivity with $C_v = 3.48 \text{ J} \cdot \text{K}^{-1} \cdot \text{cm}^{-3}$ [27]), $\kappa_{\infty} = 4.07 \text{ W} \cdot \text{cm}^{-1} \cdot \text{K}^{-1}$ is the conductivity of bulk Cu, t is the grain size, and ρ is the empirical thermal resistance of the grain boundaries. Equation (1) is obtained by assuming the thermal resistance of the grain boundaries is in series with that of the grain interior, i.e. heat must flow through both as it traverses the sample. Whether that thermal energy is carried by electrons or phonons and whether it is scattered specularly, diffusely, or some combination of both at the interface is not addressed here; the interface thermal resistance ρ represents the cumulative impact of the scattering phenomena on thermal conductivity normal to the interface. Assuming ρ to be 10^{-5} to $10^{-6} \text{ cm}^2 \cdot \text{K} \cdot \text{W}^{-1}$ [7-10] and using the data in Fig. 3, the grain size t is calculated to be approximately $3 \mu\text{m}$ to $0.3 \mu\text{m}$. These values are reasonable for the as-deposited film since grain size is usually similar to film thickness. The as-deposited grain size could not be measured experimentally due to specimen warming during preparation for viewing by transmission electron microscope (TEM).

Al/Ti Multilayers

The normal and in-plane diffusivities of the Al/Ti multilayers decrease as the bilayer thickness decreases (Fig. 5). In the plot of the normalized normal diffusivity (Fig. 5a), the experimental value approaches the predicted value as the bilayers become thicker (the ratio approaches 1.0). The properties of the material, rather than the interfaces, dominate heat flow at these thicknesses. Because heat flow normal to the layers is limited by the low diffusivity Ti, this convergence of the experimental and predicted results indicates that the properties of the $3 \mu\text{m}$ Ti films, which were used to predict the multilayer behavior, are appropriate for the multilayers. The data for in-plane diffusivity (where the Al dominates heat flow) does not approach unity, a point addressed later.

The dependence of the diffusivities on bilayer thickness (Fig. 5) is believed to arise from the interface resistance. It is clear from TEM and EELS (Fig. 4a,b) as well as microstructural studies of evaporated Ti/Al multilayer films [28] that the combined compositional diffuseness and geometrical roughness of these interfaces is less than 2 nm. The compositional diffuseness is likely related to interdiffusion as no intermetallic phases (e.g., Ti_3Al) are evident in TEM images. The impact of the grain boundaries within the layers will be discussed later.

It is proposed that the bilayer thickness impacts the normal diffusivity entirely through an interface thermal resistance (ρ) at each interface. As with the Cu films, this study does not attempt to determine the nature of scattering at the interface; the parameter ρ represents the experimentally determined impact of the scattering phenomena. In this case the thermal resistance for heat flowing through (normal to) a single bilayer can be obtained by summing the thermal resistances, thickness divided by conductivity, of the Al and Ti layers and two interfaces

$$\frac{(t_{\text{Al}} + t_{\text{Ti}})}{\kappa^{\perp}} = \frac{t_{\text{Al}} - \delta}{\kappa_{\text{Al}}} + \frac{t_{\text{Ti}} - \delta}{\kappa_{\text{Ti}}} + \frac{2\delta}{\kappa_{\text{int}}} \quad (2)$$

κ^\perp is the effective normal conductivity, the thickness of each layer has been reduced by the effective thickness δ of each interface, $\delta/2$ for the interface on each side of the layer, and κ_{int} is the conductivity of the material in the interface region.

Consistent with definitions of other interface quantities, e.g. interface free energies [30], the interface thermal resistance ρ is understood to be an *excess* thermal resistance. It is the thermal resistance in excess of that predicted using bulk properties for the region that is ascribed to the interface, whatever its thickness, i.e.

$$\rho = \delta \left(\frac{2}{\kappa_{\text{int}}} - \frac{1}{\kappa_{Al}} - \frac{1}{\kappa_{Ti}} \right) \quad (3)$$

Using Eq. 3, Eq. 2 can be rewritten

$$\frac{(t_{Al} + t_{Ti})}{\kappa^\perp} = \frac{t_{Al}}{\kappa_{Al}} + \frac{t_{Ti}}{\kappa_{Ti}} + \rho \quad (4)$$

Written in this way, the thermal transport normal to the interfaces is seen to depend on the interface thermal resistance but not the interface thickness; the effective normal conductivity κ^\perp decreases with decreasing layer thickness if there is a nonzero, positive ρ . For the specific heat of the coating, the rule of mixtures is assumed to apply to the interface region. In this case, the interface, i.e. the interface thermal resistance, is not associated with any specific heat. The specific heat per unit volume (C_{avg}) of the material, which is a scalar, is then given by the volume-weighted average

$$C_{\text{avg}} = \frac{(t_{Al} C_{Al} + t_{Ti} C_{Ti})}{(t_{Al} + t_{Ti})} \quad (5)$$

Using $\alpha^\perp = \kappa^\perp / C_{\text{avg}}$, Eqs. 4 and 5 yield the formula for the dependence of the effective normal diffusivity on the layer thickness and interface resistance,

$$\alpha^\perp = \left[\frac{t_{Al}}{\kappa_{Al}} + \frac{t_{Ti}}{\kappa_{Ti}} + 2\rho \right]^{-1} \frac{(t_{Al} + t_{Ti})^2}{(t_{Al} C_{Al} + t_{Ti} C_{Ti})} \quad (6)$$

The fact that the experimental *in-plane* diffusivity (Fig. 5b) is also a function of the layer thickness is inconsistent with a macroscopic continuum model of heat flow for layers having perfectly sharp interfaces. Such a model would predict no reduction of heat flow parallel to the layers. However, for the underlying electron and/or phonon energy transport mechanisms, even perfectly specular scattering at perfectly sharp, coherent interfaces would impact thermal transport parallel to the interfaces (Fig. 3 of Ref. [19]). However, the predictive abilities of phonon and/or electron scattering models are limited by the need to define, a priori, the scattering properties of the interface. Because these limitations are evident in comparison of

experimental and theoretical predictions (Fig. 2 of Ref. [19] for layers thicker than 7 nm), we pursue the continuum model.

An effective thickness and modified properties are ascribed to the interface region. The experimental values are expected to arise from geometrical roughness, compositional diffuseness, and/or modified band structure in the region of the interface and their impact on the underlying energy transport mechanism. For the interface thickness, as for the interface resistance, it is not necessary to understand either the scattering or transport mechanism in order to assess the impact.

For conduction parallel to interfaces of nonzero thickness, heat flows in parallel through the layers and the interface. Therefore one can obtain the total thermal flux (per unit width of bilayer) from the Ti, Al and interface regions as follows:

$$\kappa^{\parallel}(t_{Al} + t_{Ti}) = \kappa_{Al}(t_{Al} - \delta) + \kappa_{Ti}(t_{Ti} - \delta) + 2\delta\kappa_{int} \quad (7)$$

Using $\alpha^{\parallel} = \kappa^{\parallel}/C_{avg}$, Eqs. 5 and 7 yield the formula for the dependence of the in-plane diffusivity on the layer thickness, interface thickness and interface resistance,

$$\alpha^{\parallel} = \frac{\kappa_{Al}(t_{Al} - \delta) + \kappa_{Ti}(t_{Ti} - \delta) + 2\delta\kappa_{int}}{t_{Al}C_{Al} + t_{Ti}C_{Ti}} \quad (8)$$

Figure 8a shows the measured normal diffusivity data compared with values predicted by Eq. 6 (and Eq. 3 to relate ρ and κ_{int}). Figure 8b shows the measured in-plane diffusivity data compared with values predicted by Eq. 8. The same parameters were used for both predictions. They were optimized to fit the data by minimization of a weighted root-mean-square difference of the experimental and predicted values. The differences between the diffusivity data and the predicted values in the optimization were normalized by the largest experimental values, $0.07 \text{ cm}^2 \cdot \text{s}^{-1}$ (normal) and $0.3 \text{ cm}^2 \cdot \text{s}^{-1}$ (in-plane), to ensure equally good fitting of both normal and in-plane data. The Al and Ti conductivities as well as the interface thermal resistance and thickness were the free parameters in the optimization. The optimal values of the fitting parameters are as follows: $\delta = 1.5 \text{ nm}$, $\rho = 2.1 \times 10^{-6} \text{ cm}^2 \cdot \text{K} \cdot \text{W}^{-1}$, $\kappa_{Ti} = 0.091 \text{ W} \cdot \text{cm}^{-1} \cdot \text{K}^{-1}$ and $\kappa_{Al} = 1.4 \text{ W} \cdot \text{cm}^{-1} \cdot \text{K}^{-1}$.

The interface thickness $\delta = 1.5 \text{ nm}$ is in good agreement with the results of TEM and EELS (see Fig. 4a,b). The interface resistance $\rho = 2.1 \times 10^{-6} \text{ cm}^2 \cdot \text{K} \cdot \text{W}^{-1}$ is nearly identical to the value $10^{-6} \text{ cm}^2 \cdot \text{K} \cdot \text{W}^{-1}$ obtained for YSZ/SiO₂ interfaces in multilayers [10]. It is approximately an order of magnitude smaller than values obtained from metal/metal multilayers at room temperature [8] as well as upper bound values obtained at elevated temperatures [7, 9]. It is between one and two order of magnitude smaller than the range of values, between 4×10^{-4} and $5 \times 10^{-5} \text{ cm}^2 \cdot \text{K} \cdot \text{W}^{-1}$, obtained at room temperature for metal/dielectric interfaces from thin film experiments [31] (values published as interface, or Kapitza, conductance, which equals ρ^{-1}).

The conductivity κ_{Ti} is in good agreement with the value obtained from the 3 μm Ti specimen. The conductivity κ_{Al} is significantly lower than the value obtained from the 3 μm Al specimen (Table I). The reason for the discrepancy is the smaller grain boundary spacing within the Al layers of the multilayer film (see Fig. 4c). These grain boundaries lower the in-plane thermal diffusivity just as the interfaces between layers lower the normal diffusivity. Using a

grain dimension of $d = 0.1 \mu\text{m}$ (see Fig. 4c) and $\kappa_{\text{Al}} = 2.36 \text{ W} \cdot \text{cm}^{-1} \cdot \text{K}^{-1}$ (Table I), the thermal resistance across one Al grain, $d/\kappa_{\text{Al}} = 4.5 \times 10^{-6} \text{ cm}^2 \cdot \text{K} \cdot \text{W}^{-1}$, is similar to the interface thermal resistance $\rho = 2.1 \times 10^{-6} \text{ cm}^2 \cdot \text{K} \cdot \text{W}^{-1}$ just obtained. The grain boundary thermal resistance, expected to be similar in size to the interface thermal resistance, is therefore likely to decrease the diffusivity of the Al layers significantly in the multilayer specimens. A similar calculation for the Ti layers shows that the Ti grain boundaries may be safely ignored for these grain dimensions, due to the much lower conductivity of the Ti (Table I).

Our initial neglect of the grain boundaries within the Al layers has resulted in an artificially high value for the interface resistance. Because of its relatively high diffusivity and the series geometry for thermal transport normal to the film, fitting of the normal diffusivity data is not affected significantly by the properties assumed for the Al layer. Therefore, the error introduced by neglect of the Al grain boundaries can be estimated by fitting only the normal diffusivity data. Using a least squares minimization to fit Eq. 6 to only the measured normal diffusivity data with only the interface resistance as a free parameter and using the measured diffusivities of the 3 micron films yields an interface thermal resistance of $1.6 \times 10^{-6} \text{ cm}^2 \cdot \text{K} \cdot \text{W}^{-1}$. Based on this result, $2.1 \times 10^{-6} \text{ cm}^2 \cdot \text{K} \cdot \text{W}^{-1}$ is an upper bound for the interface thermal resistance $\rho = 1.6 \times 10^{-6} \text{ cm}^2 \cdot \text{K} \cdot \text{W}^{-1}$.

From comparison of Figs. 5b and 6, it is clear that the in-plane thermal diffusivity is less sensitive to the decrease of layer thickness (decreasing by a factor of 2) than the electrical conductance (decreasing by a factor of 6). We thus conclude that the fraction of total in-plane energy transported by electron conduction decreases with decreasing layer thickness. Phonon conduction is presumed to account for the remainder. That the electrical conductivity is still increasing with layer thickness, even for the multilayers with the thickest layers, is consistent with the sub-unity value of the normalized in-plane thermal diffusivity at these thicknesses (Fig. 5b).

Conclusions

The thermal diffusivities of Cu, Al and Ti thin films on substrates and Al/Ti multilayer thin films on substrates have been measured using the Mirage technique. Copper films 0.5 to 5 μm thick were found to possess essentially isotropic thermal diffusivities that were within 10% of bulk values; annealing reduced this difference to approximately 5% for the thicker films. The Al and Ti films exhibited isotropic bulk properties. The Al/Ti multilayer films exhibited a substantial decrease of thermal diffusivity below that predicted based on bulk materials for thermal transport both in the plane of, and normal to, the layers. The clear dependence of both the in-plane and normal diffusivities on the bilayer thickness was used to determine the interface resistance ($\rho = 1.6 \times 10^{-6} \text{ cm}^2 \cdot \text{K} \cdot \text{W}^{-1}$) of this metal/metal multilayer system. This value is somewhat smaller than values previously reported for metal/metal interfaces. Electrical measurements demonstrate that the in-plane electrical conductance, like the in-plane thermal diffusivity, decreases with decreasing layer thickness. However, it does so far more rapidly.

Acknowledgements

This work was supported in part by NIST's Advanced Technology Program.

References

1. J. C. Lambropoulos, M. R. Jolly, C. A. Amsden, S. E. Gilman, M. J. Sinicropi, D. Diakomihalis, and S. D. Jacobs, *J. Appl. Phys.* **66**, 4230 (1989).
2. A. J. Griffin, Jr., F. R. Brotzen, and P. J. Loos, *J. Appl. Phys.* **75**, 376 (1994).
3. A. J. Griffin, Jr., F. R. Brotzen, and P. J. Loos, *J. Appl. Phys.* **76**, 450 (1994).
4. S. M. Lee, D. G. Cahill, *J. Appl. Phys.* **81** (6), 2590 (1997).
5. E.T. Swartz and R.O. Pohl, *Reviews of Modern Physics* **61**, 605 (1989).
6. D.G. Cahill, *Microscale Thermophysical Engineering* **1**, 85 (1997).
7. D. Josell, A. Cezairliyan, D. van Heerden and B.T. Murray, *Internat. J. Thermophys.* **18**, 865 (1997).
8. B.M. Clemens, G.L. Eesley and C.A. Paddock, *Phys. Rev. B* **37**, 1085 (1988).
9. D. Josell, A. Cezairliyan and J.E. Bonevich, *Internat. J. Thermophys.* **19**, 525 (1998).
10. S.-M. Lee, G. Matamis, D.G. Cahill, W.P. Allen, *Microscale Thermophysical Engineering* **3**, 31 (1998).
11. T. Yao, *Appl. Phys. Lett.* **51**, 1798 (1987).
12. Z. C. Zhang, J.P. Roger, D. Fournier, A.C. Boccara and J.C. Wang, *Thin Solid Films* **186**, 361 (1990).
13. X.Y. Yu, G. Chen, A. Verma and J.S. Smith, *Appl. Phys. Lett.* **67**, 3554 (1995).
14. S.-M. Lee, D.G. Cahill, R. Venkatasubramanian, *Appl. Phys. Lett.* **70**, 2957 (1997).
15. G. Chen, C.L. Tien, X. Wu, J.S. Smith, *J. Heat Transfer* **116**, 325 (1994).
16. W.S. Capinski, H.J. Maris, T. Ruf, M. Cardona, K. Ploog, D.S. Katzer, *Phys. Rev. B* **59**, 8105 (1999).
17. R.J. Stoner and H.J. Maris, *Phys. Rev. B* **48**, 16373 (1993).
18. G. Chen, *J. Heat Transfer* **119**, 220 (1997).
19. G. Chen and M. Neagu, *Appl. Phys. Lett.* **71**, 2761 (1997).
20. P. K. Kuo, E. D. Sandler, L. D. Farvo, and R. L. Thomas, *Can. J. Phys.* **64**, 1168, 1986.
21. L. Wei, Ph.D. Dissertation, Wayne State University, Detroit, MI (1992).
22. L. Wei, M. Vaudin, C. S. Hwang, and G. White, *J. Mater. Res.* **10**, 1889 (1995).
23. D. Josell, E.J. Gonzalez, and G.S. White, *J. Mater. Res.* **13**, 1117 (1998).
24. E. J. Gonzalez, G. White, and L. Wei, *J. Mater. Res.* (in press).
25. E. J. Gonzalez, B. Hockey, and J. J. Ritter (private communication).
26. Y. S. Touloukian, R. W. Powell, C. Y. Ho, and M. C. Nicolaou, *Thermophysical Properties of Matter*, Vol. 10, Plenum Publishing, New York, (1973).
27. Y. S. Touloukian, and E. H. Buyco, *Thermophysical Properties of Matter*, Vol. 5, Plenum Publishing, New York, (1970).
28. J. Bonevich, D. van Heerden, and D. Josell, *J. Mater. Res.* **14**, 1977 (1999).
29. L.B. Valdes, *Proc. IRE* **42**, 420 (1954).
30. J.W. Cahn, in *Interfacial Segregation*, Eds. W.C. Johnson and J.M. Blakely, ASM Seminar (1978), pp. 3-23.
31. S.-M. Lee and D.G. Cahill, *Microscale Thermophysical Engineering* **1**, 47 (1997).

Table I. Selected Properties of Al and Ti bulk and 3.0 μm thick films at ~ 300 K

Thermophysical Property	Bulk Al	Measured Al Film*	Bulk Ti	Measured Ti Film*
Specific Heat ($\text{J} \cdot \text{cm}^{-3} \cdot \text{K}^{-1}$) [27]	2.44	2.44	2.35	2.35
Thermal Diffusivity ($\text{cm}^2 \cdot \text{s}^{-1}$) [26]	0.968	0.968 ± 0.012	0.0925	0.035 ± 0.003
Thermal Conductivity ($\text{W} \cdot \text{cm}^{-1} \cdot \text{K}^{-1}$)	2.36	2.36 ± 0.03	0.217	0.082 ± 0.006

*Films were deposited under conditions identical to those used for the multilayers (nominal thickness also 3.0 μm). Thermal conductivity is calculated from the measured thermal diffusivity using the specific heat of the bulk materials.

Table II. Properties of Al/Ti Multilayer Specimens

Physical Parameter	37 Bilayers Al/Ti	75 Bilayers Al/Ti	150 Bilayers Al/Ti	300 Bilayers Al/Ti	600 Bilayers Al/Ti
Al vol.%	50	49	49	42	45
Bilayer Thickness (nm)	80	40.7	21	10.4	5.0
Total Thickness (μm)	3.00	3.05	3.15	3.12	3.30

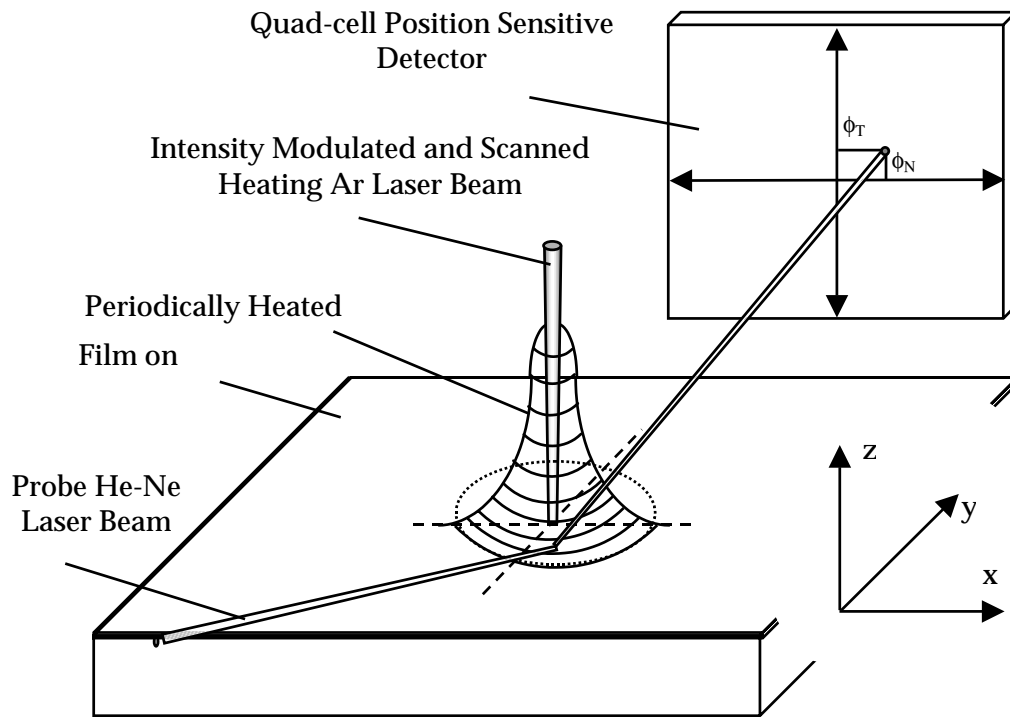


Figure 1: Configuration of the Mirage experimental setup. The source beam is surrounded by a region of air heated, principally, according to the temperature profile on the specimen surface. The probe beam is shown being deflected by the heated air and impinging on the detector used to determine the magnitude and phase lags of the normal (ϕ_n) and transverse (ϕ_t) deflections. Data is acquired as the probe beam is moved along the x direction. The two components of the probe beam deflection are greatly exaggerated.

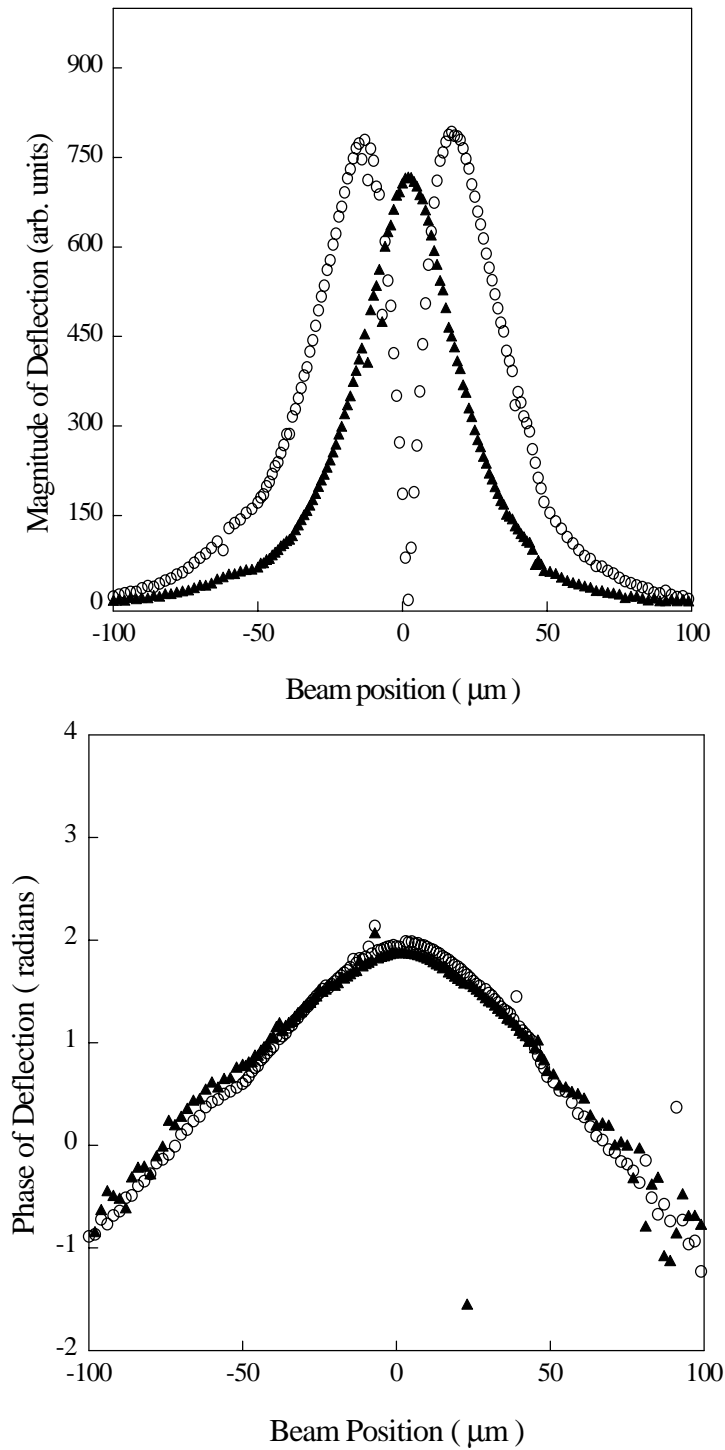


Figure 2: (a) The magnitudes of the normal (solid triangle) and transverse (open circle) deflections of the probe beam as functions of the horizontal distance between the probe and source beams. Note that the symmetry of the geometry requires that the transverse deflection equals zero if the probe beam passes through the source beam. (b) The phase lag of the normal (solid triangle) and transverse (open circle) deflections of the probe beam as functions of the horizontal distance between the probe and source beams

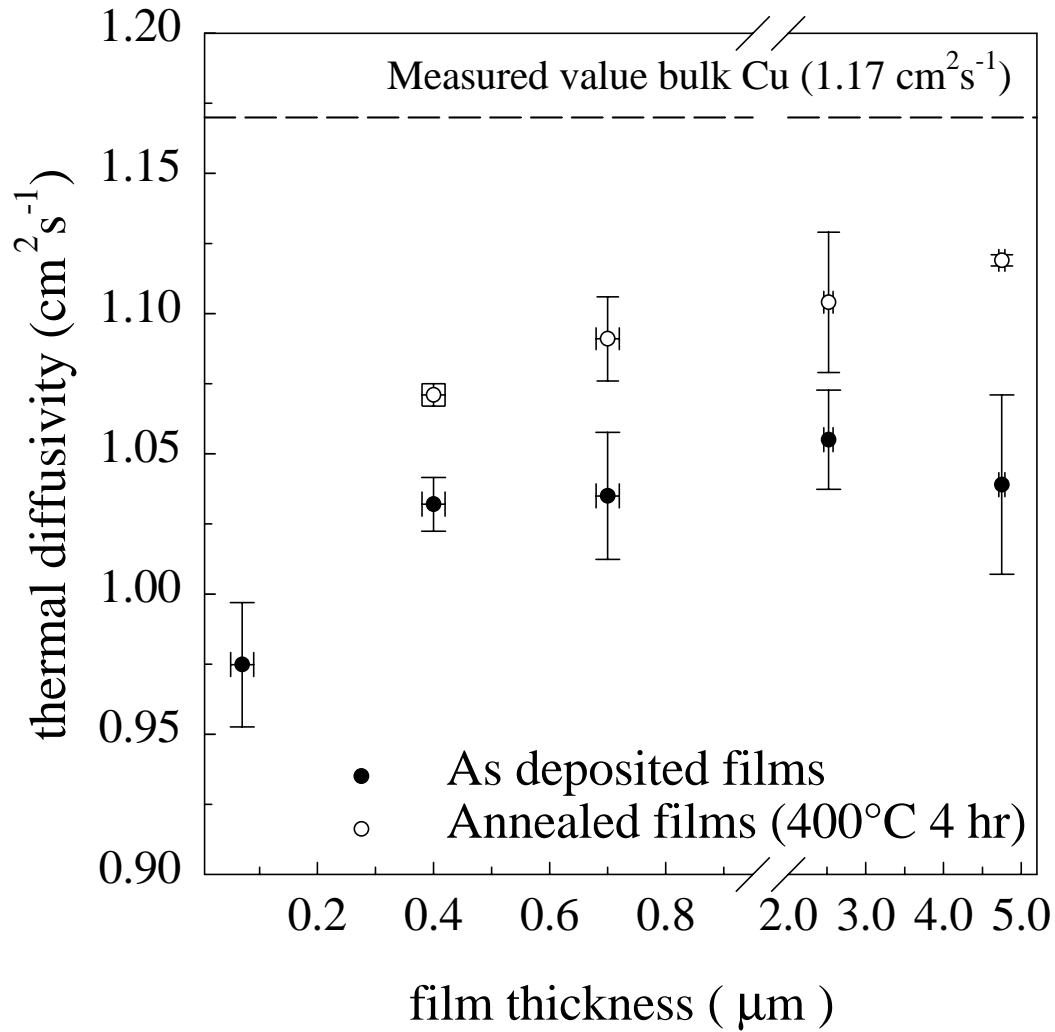


Figure 3: Room temperature thermal diffusivity data acquired for the Cu thin films on quartz. The solid circles indicate the measured diffusivities of the as-deposited specimens. The open circles indicate the measured diffusivities of the specimens annealed for four hours at 400°C . The $0.1 \mu\text{m}$ thick specimen was not studied in the annealed state because of oxidation.

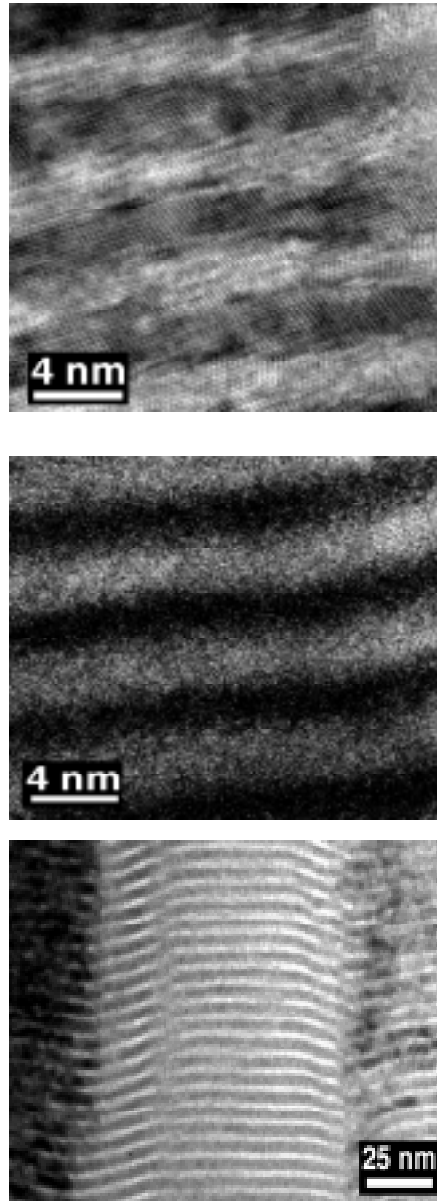


Figure 4: (a) Transmission electron micrograph of Al/Ti multilayer with nominally 2.5 nm thick layers. (b) Compositional map, with intensity proportional to Ti content, obtained by electron energy loss spectroscopy (EELS). (c) Grain structure as viewed by TEM.

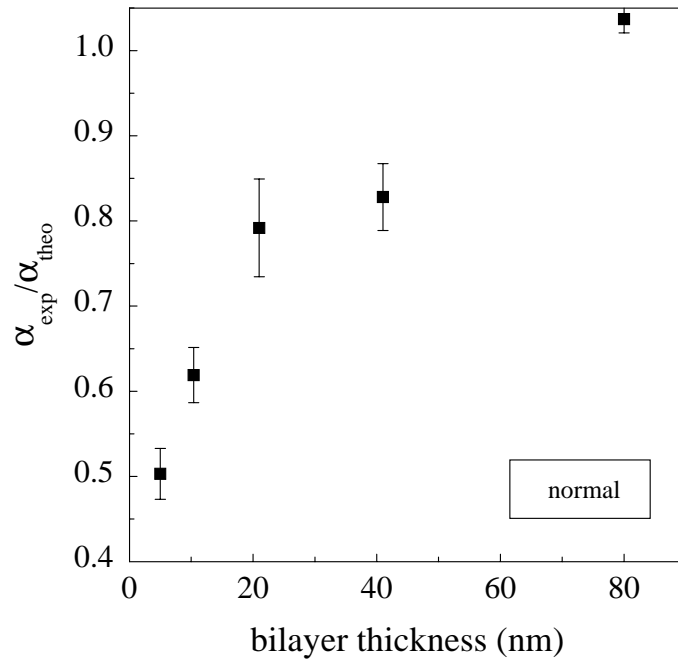
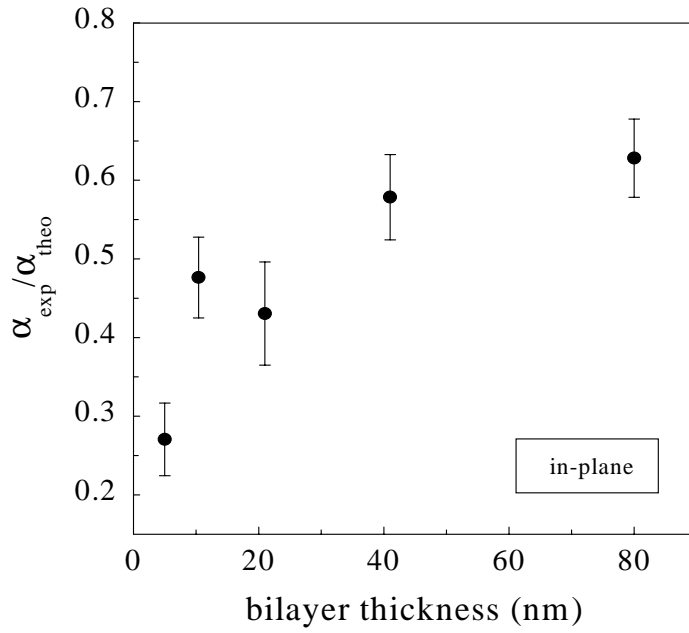


Figure 5: (a) The measured normal thermal diffusivities of the Al/Ti multilayers normalized by the values predicted based on the series nature of the layers using Al and Ti diffusivities obtained from the 3 μm thick films. (b) The measured in-plane thermal diffusivities of the Al/Ti multilayers normalized by the values predicted based on the parallel nature of the layers using Al and Ti diffusivities obtained from the 3 μm thick films.

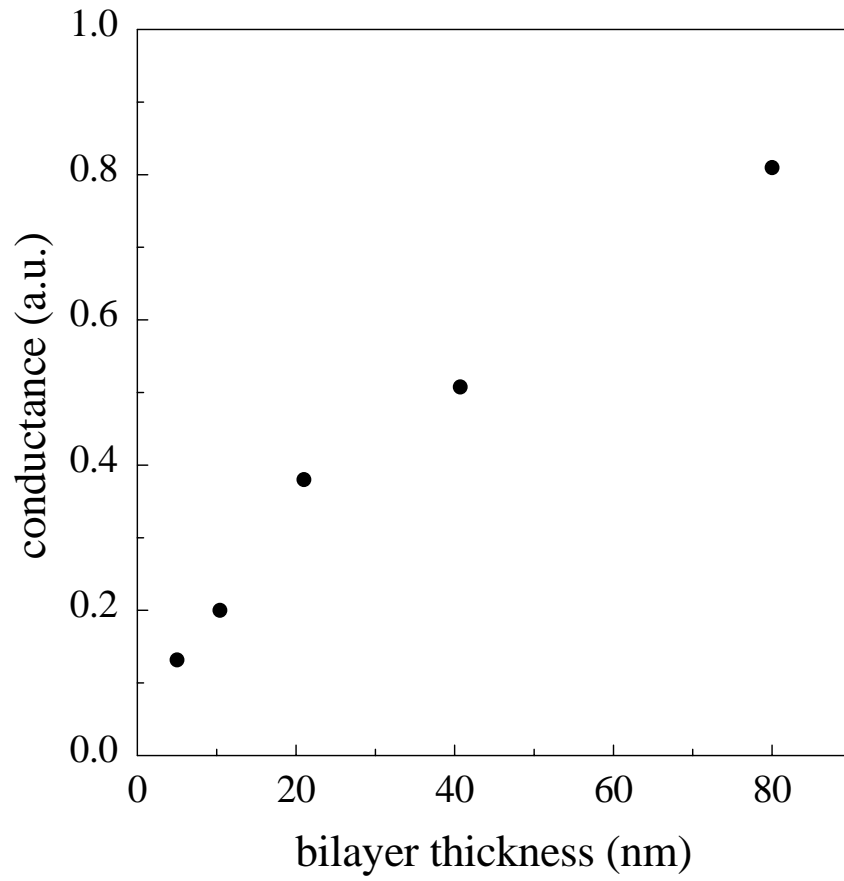


Figure 6: The measured in-plane electrical conductances of the Al/Ti multilayers in arbitrary units.

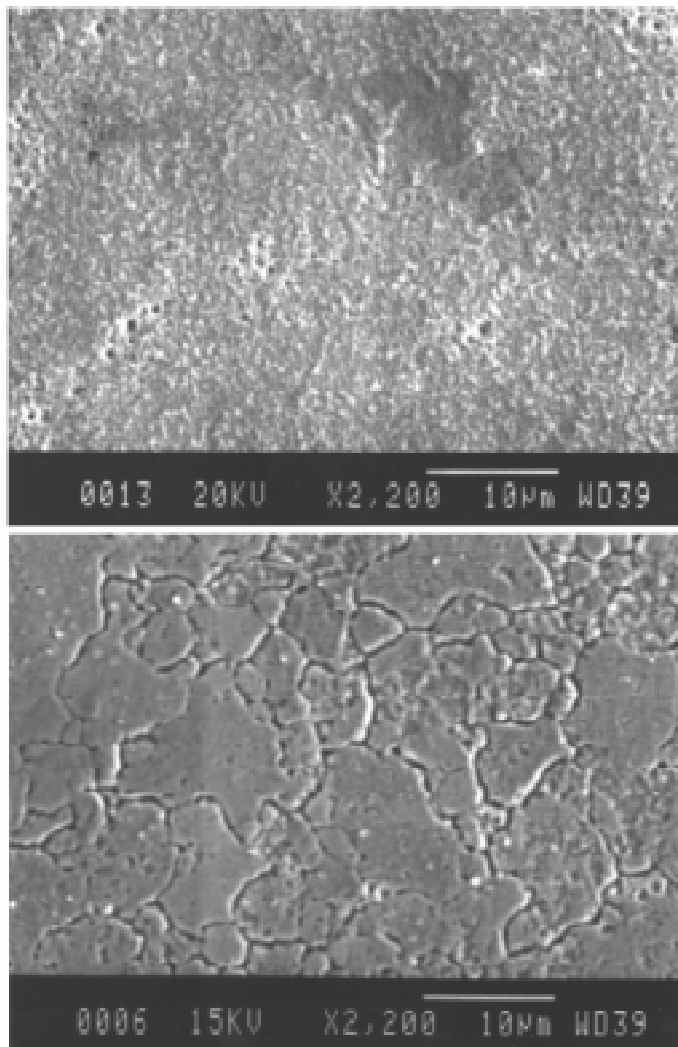


Figure 7: Scanning electron micrographs showing the surfaces of the 5 μm thick Cu film: (a) as-deposited and etched, (b) annealed and etched. Note the large grains evident in the annealed specimen.

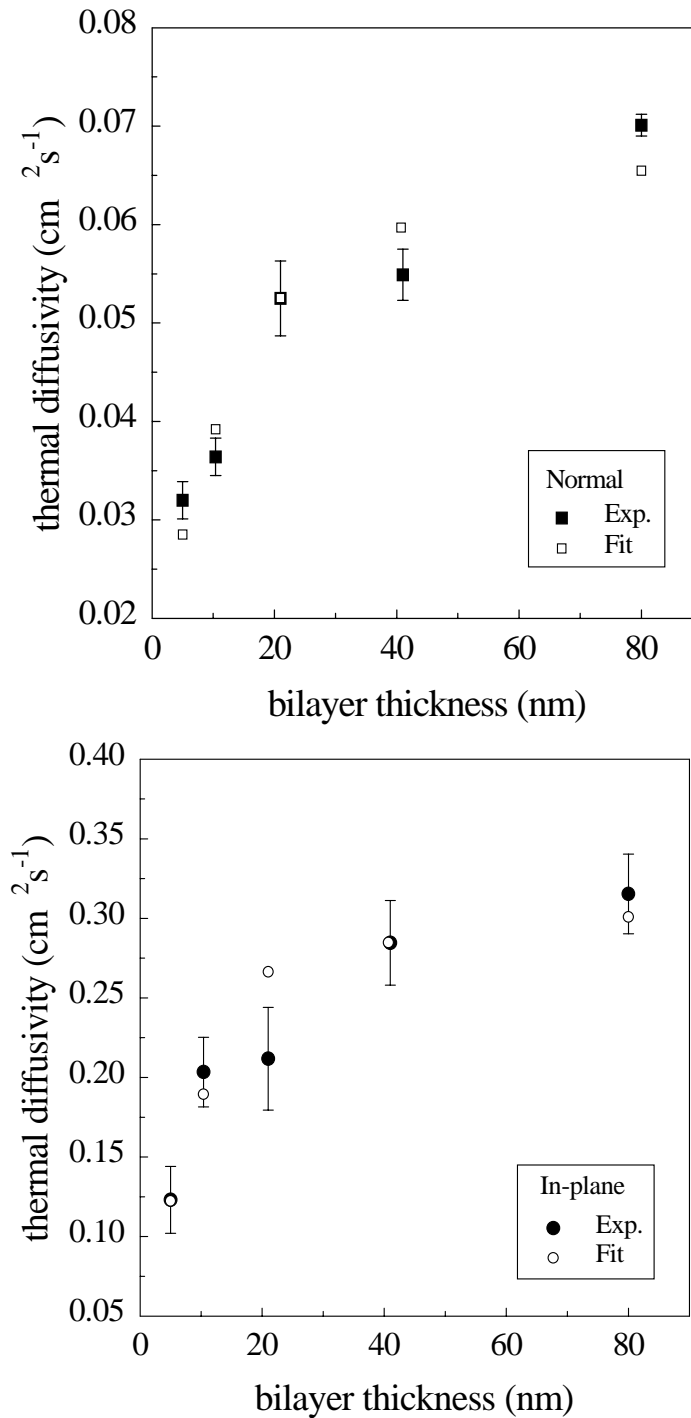


Figure 8: (a) The measured normal thermal diffusivities of the Al/Ti multilayers (solid square) compared with the values predicted based on Eq. 4 (open square). (b) The measured in-plane thermal diffusivities of the Al/Ti multilayers (solid circle) compared with the values predicted based on Eq. 6 (open circle).